Signal Analysis for an Entomological Radar with a Vertical Nutating Beam

College of Aeronautics Report 9919

ISBN 1 86194 0483

Dr. S.E. Hobbs
College of Aeronautics
Cranfield University, Cranfield, Bedford, MK43 0AL

K. Allsopp
School of Industrial and Manufacturing Science
Cranfield University, Cranfield, Bedford, MK43 0AL

W.Wolf
United States Department of Agriculture
College Station, Texas, USA

15 March 2000, 19 Sept 2003

Signal Analysis for an Entomological Radar with a Vertical Nutating Beam

College of Aeronautics Report 9919
ISBN 1 86194 0483

S.E. Hobbs, K. Allsopp, W.Wolf

Abstract

This report documents the signal analysis procedures developed at Cranfield University for ground based entomological radars. The radars use a nutating vertical beam, allowing target (individual insect) position and radar cross-section (RCS) parameters to be measured

The model accounts for non-circular beam cross-sections and assumes a three parameter target RCS model. An iterative maximum-likelihood algorithm is used, and uses the model and system noise data to provide quantitative measures of the model's goodness of fit to the data and of parameter uncertainties as well as the best fit solution parameters.

Successful applications of the algorithm to both radar calibration and insect monitoring are illustrated with field observations using the USDA/Cranfield ground-based entomological radar system. The results show good performance for the analysis method, but do not exploit its full potential because the noise model is only approximate.

Contents

List of Figures

List of Tables

Notation

a	antenna radius
$\mathbf{a}$	vector of model parameters
ADC	analogue to digital converter
b	beam deviation factor
c	radar system constant (signal for the calibration sphere on axis at the reference range)
d	antenna diameter
DN	digital number (e.g. the ADC output value)
E	electric field strength
f	antenna focal length
$F(\theta, \phi)$	antenna response function
g_i	beam cross-section parameters ($i = 1, 2$)
I	field intensity in radar beam (one-way)
$J_1()$	first order Bessel function of the first kind
k	radar system constant in the Radar Equation
p	radar system signal (log receiver assumed)
P_r	received power at the radar
P_{r0}	received power at the radar for reference target
q	beam shape coordinate ($= \sin\theta/\lambda$)
R	slant range distance from radar to target
R_0	slant range to reference target
S_{0-4}	Fourier signal integrals used to obtain first guess for solution
t	time
u	angular velocity component along x axis
v	angular velocity component along y axis
x	angular position coordinate of target ($= X/R$)
x_0	$x_0 = x(t = 0)$
X	(linear) position coordinate of target wrt nutation axes
X_0	position coordinate at $t = 0$
y	angular position coordinate of target ($= Y/R$)
y_0	$y_0 = y(t = 0)$
Y	(linear) position coordinate of target wrt nutation axes
Y_0	position coordinate at $t = 0$

Table 1: Symbols (Roman) used in the report.

α	azimuth of beam centre around nutation axis
α_0	beam centre azimuth at $t = 0$
β	phase angle in target scattering matrix
γ_i	beam width along principal axes of elliptical cross-section ($i = 1, 2$)
δ	dipole eccentricity in antenna (radius of eccentric motion)
ϵ	ratio of principal cross-sections in target scattering matrix
λ	wavelength (of the radio frequency radiation)
ρ	polarisation direction in nutation axes (parallel to electric field)
ρ_0	polarisation direction at $t = 0$
ρ_r	polarisation angle relative to target orientation
ρ_{r0}	ρ_r at $t = 0$
θ	target radial angular displacement from beam axis (beam coordinates)
$\theta_{1/2}$	one-way half-power beam radius
θ'	beam centre angular displacement from nutation axis
θ''	target radial angular displacement from nutation axis
ϕ	target azimuth around beam axis
ϕ'	angular offset between principal axis of beam cross-section and radius from nutation axis to beam axis
ϕ''	target azimuth around nutation axis
σ	target radar cross-section
σ	measurement uncertainty (noise), which may depend on signal power
σ_{xx}	target radar cross-section for transmit and receive polarisations parallel to body axis
σ_0	radar cross-section of reference target (e.g. steel sphere)
χ	(insect) target orientation about nutation axis
χ^2	statistic used to determine the quality of the fit between the model and the data
χ_0^2	χ^2 when the "model" is just the mean signal. χ_0^2 is a reference value with which the model χ^2 can be compared.
ψ	target azimuth about nutation axis relative to beam centre ($= \phi'' - \alpha$)
ω	nutation (and polarisation) angular velocity

Table 2: Symbols (Greek) used in the report.

Chapter 1

Introduction

Ground based radars have been used for over 25 years to monitor insect flight. Early scanning radars gave dramatic information about insect migration, but were unable to identify individual targets because their position in the radar beam, and thus their absolute radar backscatter cross-section (RCS), could not be measured. Vertically-looking radars using a nutating beam (the beam is offset slightly from the vertical and rotates around the vertical axis) provide the information required to measure absolute position and RCS for individual targets, opening new possibilities in radar entomology. The nutating beam method has been used in radar entomology for a number of years by research groups based in the UK, Australia and the USA [1].

A good model of the radar system is needed for effective data analysis able to extract the information available from the measurements. In particular, the aim is to measure the trajectory of the insects (position, heading, velocity, orientation) and radar cross-section. The system model and solution algorithm described here account for non-circular beam cross-sections and use a three parameter target RCS model. This RCS model is suitable for targets with a plane of symmetry which includes the viewing direction - as is the case for an insect flying horizontally and viewed from vertically below (or above).

The model has several possible applications:

- Routine data analysis
- System calibration
- System design

The first two applications are the main subject of this report. System design is also an important application because having a good model allows the effect on performance of varying system parameters to be studied quantitatively.

A maximum likelihood solution method is used. This has the advantages of

1. quantifying the goodness of fit of the model to the data,
2. if the fit is good enough then the best fit solution parameters are obtained,
3. quantitative parameter uncertainty covariances are calculated.

Standard non-linear optimisation routines can be used to find the solution.

The report covers the analytical model developed at Cranfield, its incorporation into a maximum likelihood solution algorithm, and some example applications. Chapter 2 documents the analytical model which takes account of the radar beam geometry and the target's radar cross-section. Chapter 3 discusses how this model can be incorporated into a maximum likelihood algorithm to estimate model parameters given radar measurements (and their uncertainties). Chapter 4 illustrates the method with examples of results obtained from experiments performed in November 1988 with the US Department of Agriculture. The final chapter briefly discusses the main features of the method and its use in radar entomology.

Chapter 2

Model of the Radar System

A model of a nutating beam entomological radar has been developed. The model has three main elements:

1. the standard radar equation,
2. the beam geometry
3. the insect radar cross-section

Each of these elements is described in turn and then all are combined to develop the complete model. The next chapter describes how the model is used to analyse measured signals, and the solution algorithm used to estimate model parameters.

2.1 The Radar Equation

The radar equation for point targets, which gives the returned power (P_r) in terms of the target's radar cross-section (σ), the beam cross-section function ($F(\theta, \phi)$, where θ, ϕ describe the target's position in the beam in terms of the radial and azimuthal angles respectively), the target's range (R), and a constant (k) depending on the radar transceiver's characteristics is

$$P_r = k\frac{\sigma F^4(\theta, \phi)}{R^4} \tag{2.1}$$

To avoid the difficulty of measuring k directly, Equation 2.1 can be rewritten in terms of the power received (P_{r0}) from a target of known radar cross-section (σ_0) at at known range (R_0) on the beam axis ($F = 1$).

$$\frac{P_r}{P_{r0}} = \frac{\sigma F^4(\theta, \phi) R_0^4}{\sigma_0 R^4} \tag{2.2}$$

For the nutating beam system modelled here (Figure 2.1), the beam shape function and radar cross-section are described in detail using the following models.

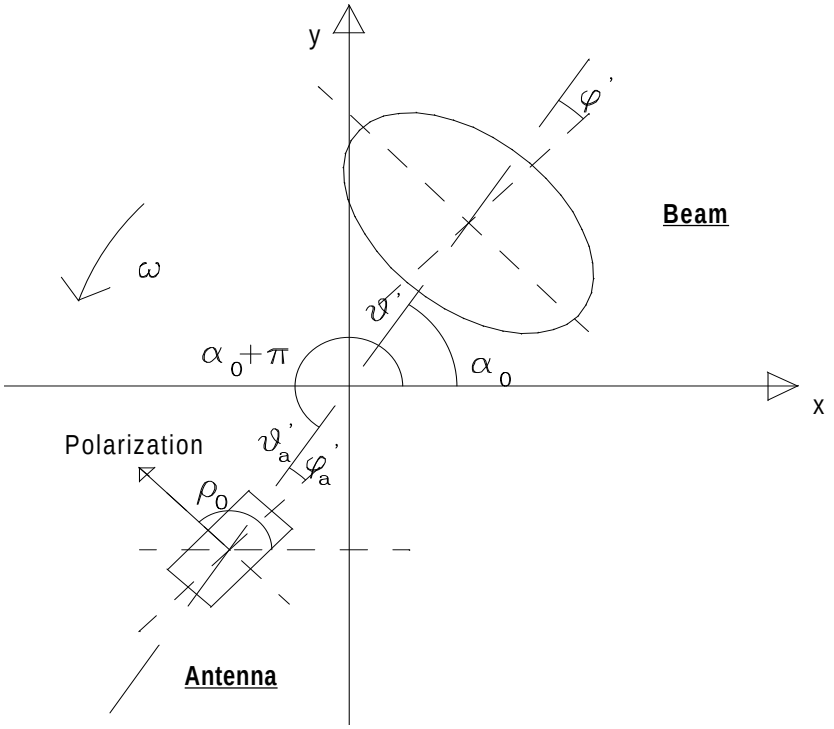

Figure 2.1: Elliptical radar beam geometry and the related offset dipole position (shown by the rectangular waveguide cross-section) at $t = 0$.

2.2 Beam Shape Function

A model of the beam shape is required to predict the incident field at the target's position and to calculate the fraction of the scattered power collected by the receiving antenna. For a monostatic system, the same function describes both these processes.

2.2.1 The Gaussian Approximation for the Beam Shape

An exact solution of the electric field amplitude for a uniformly illuminated circular (or elliptical) aperture involves Bessel functions. Bessel functions are less convenient to use than alternatives such as the Gaussian, and so the beam is modelled as Gaussian with an elliptical cross-section. A Gaussian is a good approximation to the exact beam shape for a circular aperture given by the usual Bessel function expansion (Table 2.1), but is appropriate for the main lobe only. Note that the values derived here apply to a circular aperture. These results can be generalised to an elliptical cross-section as is done below.

The far field electric field vector for a uniformly-illuminated circular aperture of radius a (diameter $d = 2a$), with radiation of wavelength λ, at angle θ to the

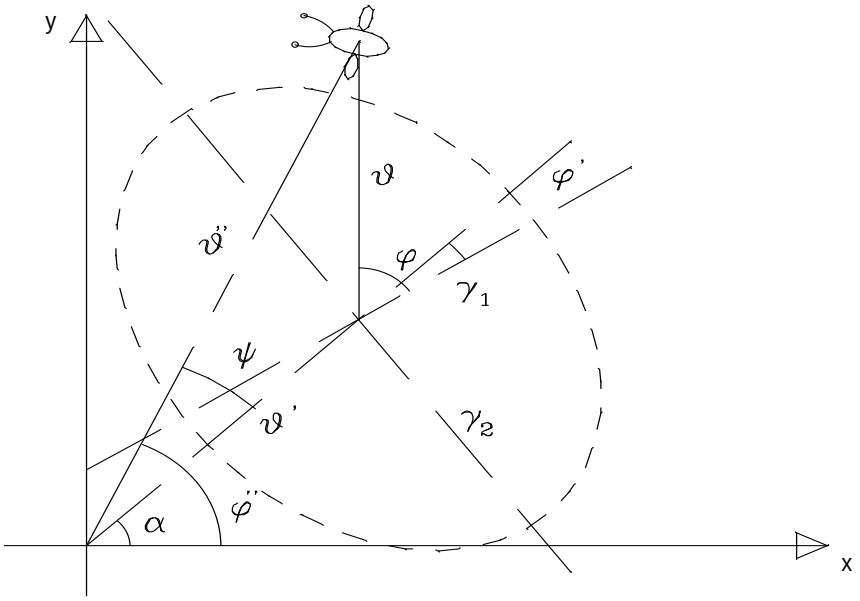

Figure 2.2: Target position relative to the beam axes and fixed system axes. Note that the radial displacements $(\theta, \theta', \theta'')$ are expressed as angles by dividing by the target range.

beam axis is given by [2]

$$E(\theta) \quad = \quad E_0 \frac{2J_1(x)}{x} \tag{2.3}$$

where $x = 2\pi aq = \pi dq = \pi d \sin\theta/\lambda$, and $J_1(x)$ is the first order Bessel function of the first kind. The corresponding Gaussian approximation for a circular aperture uses a single beam-width parameter γ:

$$E'(\theta) \quad = \quad E_0 e^{-\theta^2/\gamma^2} \tag{2.4}$$

These two models are usually related by choosing γ such that the one-way half peak intensity beamwidths are equal. Thus

$$\frac{I(\theta_{1/2})}{I_0} \quad = \quad \left(\frac{E(\theta_{1/2})}{E_0}\right)^2 \tag{2.5}$$

$$= \quad 0.5$$

$$= \quad \left(\frac{2J_1(x_{1/2})}{x_{1/2}}\right)^2 \tag{2.6}$$

This can be solved numerically, giving $x_{1/2} = 1.61634$, and then

$$\theta_{1/2} \quad = \quad \sin^{-1}\left(x_{1/2}\frac{\lambda}{\pi d}\right) \tag{2.7}$$

Angle off-axis θ	θ	Bessel I/I_0	Gaussian I/I_0	Discrepancy Gaussian - Bessel (absolute)	Gaussian ÷ Bessel (dB)	Remarks
rad	deg					
0.008	0.50	0.939	0.936	-0.003	-0.02	
0.017	1.00	0.775	0.767	-0.008	-0.04	
0.027	1.62	0.500	0.500	0.000	0.00	half-power point
0.032	1.88	0.381	0.390	0.009	0.10	0.1 dB error
0.033	1.92	0.365	0.376	0.010	0.12	1% absolute error
0.044	2.59	0.134	0.169	0.035	1.00	1 dB error
0.065	3.83	0	0.020	0.020	∞	first null

Table 2.1: Limits of validity of the Gaussian beam model. The corresponding off-axis angles are evaluated for a circular aperture of diameter 0.6 m and radar frequency of 9.4 GHz ($\gamma = 0.04646$ rad).

For the Gaussian model

$$\frac{I'(\theta_{1/2})}{I_0} = \left(\frac{E'(\theta_{1/2})}{E_0}\right)^2 \tag{2.8}$$

$$= 0.5$$

$$= e^{-2\theta_{1/2}^2/\gamma^2} \tag{2.9}$$

Thus

$$\gamma = \sqrt{\frac{2}{\ln 2}}\theta_{1/2} \tag{2.10}$$

$$= \sqrt{\frac{2}{\ln 2}}\sin^{-1}\left(x_{1/2}\frac{\lambda}{\pi d}\right) \tag{2.11}$$

Table 2.1 shows how far away from the beam axis the Gaussian approximation may be taken to be valid using various criteria.

2.2.2 Beam Shape Model using the Gaussian Approximation

The beam shape function (F) based on the Gaussian approximation gives the one-way amplitude variation of the electric field relative to its strength on the beam axis.

$$F(\theta,\phi) = \exp\left[-\left(\frac{p^2}{\gamma_1^2}+\frac{q^2}{\gamma_2^2}\right)\right] \tag{2.12}$$

$$= \exp\left[-\left(\frac{(\theta\cos\phi)^2}{\gamma_1^2}+\frac{(\theta\sin\phi)^2}{\gamma_2^2}\right)\right] \tag{2.13}$$

$$= \exp\left[-\theta^2\left(\frac{\gamma_1^2+\gamma_2^2}{2\gamma_1^2\gamma_2^2}+\frac{\gamma_2^2-\gamma_1^2}{2\gamma_1^2\gamma_2^2}\cos 2\phi\right)\right] \tag{2.14}$$

$$= \exp\left[-\theta^2\left(g_1+g_2\cos 2\phi\right)\right] \tag{2.15}$$

where

$$g_1 = \frac{\gamma_1^2 + \gamma_2^2}{2\gamma_1^2\gamma_2^2} \tag{2.16}$$

$$g_2 = \frac{\gamma_2^2 - \gamma_1^2}{2\gamma_1^2\gamma_2^2} \tag{2.17}$$

and

$$\gamma_1^2 = \frac{1}{g_1 + g_2} \tag{2.18}$$

$$\gamma_2^2 = \frac{1}{g_1 - g_2} \tag{2.19}$$

γ_1, γ_2 are the beamwidths along axes 1 and 2 of the elliptical beam cross-section (Figure 2.2). Equation 2.11 shows how the wavelength of the radiation and the aperture diameter are related to γ for a uniformly illuminated circular aperture. This provides a good first guess for the values of γ_1, γ_2.

The cosine and sine rules applied to Figure 2.2 give θ^2 and $\cos 2\phi$ in terms of the angles in a fixed frame of reference:

$$\theta^2 = \theta'^2 - 2\theta'\theta'' \cos\psi + \theta''^2 \tag{2.20}$$

$$\frac{\theta''}{\sin(\phi' + \pi - \phi)} = \frac{\theta'}{\sin(\phi - \phi' - \psi)} \tag{2.21}$$

$$\theta'' \sin(\phi - \phi' - \psi) = \theta' sin(\phi - \phi') \tag{2.22}$$

$$\sin\phi\,[\theta' \cos\phi' - \theta'' \cos(\phi' + \psi)] = \cos\phi\,[\theta' \sin\phi' - \theta'' \sin(\phi' + \psi)] \tag{2.23}$$

$$\cos 2\phi = \frac{\theta'^2 \cos 2\phi' - 2\theta'\theta'' \cos(2\phi' + \psi) + \theta''^2 \cos 2(\phi' + \psi)}{\theta'^2 - 2\theta'\theta'' \cos\psi + \theta''^2} \tag{2.24}$$

where

$$\alpha = \alpha_0 + \omega t \tag{2.25}$$

$$\psi = \phi'' - \alpha \tag{2.26}$$

$$= \phi'' - \alpha_0 - \omega t \tag{2.27}$$

Hence the beam shape function is

$$\begin{aligned} F &= F(\theta', \phi', \theta'', \phi'', \alpha_0, \omega; t) \\ &= \exp\left[\begin{array}{l} -g_1(\theta'^2 - 2\theta'\theta'' \cos\psi + \theta''^2) \\ -g_2 \left(\begin{array}{l} \theta'^2 \cos 2\phi' - 2\theta'\theta'' \cos(2\phi' + \psi) \\ +\theta''^2 \cos 2(\phi' + \psi) \end{array} \right) \end{array} \right] \end{aligned} \tag{2.28}$$

$$\begin{aligned} \ln F &= -\theta'^2(g_1 + g_2 \cos 2\phi') \\ &\quad +2\theta'\theta'' \left(g_1 \cos\psi + g_2 \cos(2\phi' + \psi)\right) \\ &\quad -\theta''^2 \left(g_1 + g_2 \cos 2(\phi' + \psi)\right) \end{aligned} \tag{2.29}$$

$$\begin{aligned} &= -4\theta'^2(g_1 + g_2 \cos 2\phi') - 4\theta''^2 g_1 \\ &\quad +8\theta'\theta'' \cos\omega t \left[g_1 \cos(\phi'' - \alpha_0) + g_2 \cos(2\phi' + \phi'' - \alpha_0)\right] \\ &\quad +8\theta'\theta'' \sin\omega t \left[g_1 \sin(\phi'' - \alpha_0) + g_2 \sin(2\phi' + \phi'' - \alpha_0)\right] \\ &\quad -4\theta''^2 \cos 2\omega t g_2 \cos 2(\phi' + \phi'' - \alpha_0) \\ &\quad -4\theta''^2 \sin 2\omega t g_2 \sin 2(\phi' + \phi'' - \alpha_0) \end{aligned} \tag{2.30}$$

The target's position and velocity are described in fixed Cartesian axes, where X and Y are the target's position in absolute units, by

$$\begin{aligned} x &= X/R \\ &= x_0 + ut \quad (2.31) \\ &= \theta'' \cos\phi'' \quad (2.32) \\ y &= Y/R \\ &= y_0 + vt \quad (2.33) \\ &= \theta'' \sin\phi'' \quad (2.34) \end{aligned}$$

thus

$$\begin{aligned} \theta'' &= \sqrt{x^2 + y^2} \quad (2.35) \\ \phi'' &= \tan^{-1} y/x \quad (2.36) \end{aligned}$$

The signs of x and y are used to determine the correct quadrant for ϕ'', i.e. if $x < 0$ then add π to the value of ϕ'' to translate it from the original range $(-\pi/2 \leq \phi'' \leq \pi/2)$ given by the function $\tan^{-1}$.

Note that equations 2.31 and 2.33 could easily be extended to include acceleration terms.

2.2.3 Beam Deviation Factor

The beam shape model requires the angular offset of the beam axis from the rotation axis (θ'). This is difficult to measure accurately in practice, but it is feasible to measure the antenna eccentricity (δ, side-to-side motion 2δ) in the reflector (focal length f). A beam deviation factor (b) is defined which relates these two offsets [3]

$$b = \frac{\theta'}{\delta/f} \quad (2.37)$$

b is a function of the reflector's focal length to diameter ratio (f/d), and is approximately 0.76 for a reflector with $f/d = 0.25$ (as is the case for the data used later in this report).

2.3 Target Radar Cross-Section

The target is assumed to have a plane of symmetry including the line of sight from the radar antenna to the target, and is thus modelled using a diagonalised form of the scattering matrix. This assumption is reasonable for radars viewing vertically, but not in general for off-vertical view directions. Figure 2.3 shows the geometry used to determine the target's RCS polarization dependence.

$$\begin{aligned} \sigma &= |(\cos\rho_r, \sin\rho_r) \begin{pmatrix} \sqrt{\sigma_{xx}} & 0 \\ 0 & \epsilon\sqrt{\sigma_{xx}} e^{i\beta} \end{pmatrix} \begin{pmatrix} \cos\rho_r \\ \sin\rho_r \end{pmatrix}|^2 \quad (2.38) \\ &= \sigma_{xx} \left(\cos^4\rho_r + 2\epsilon\cos\beta\cos^2\rho_r\sin^2\rho_r + \epsilon^2\sin^4\rho_r\right) \quad (2.39) \\ &= \frac{\sigma_{xx}}{4} \begin{bmatrix} 1 + 2\epsilon\cos\beta + \epsilon^2 + 2\cos 2\rho_r(1-\epsilon^2) \\ + \cos^2 2\rho_r(1 - 2\epsilon\cos\beta + \epsilon^2) \end{bmatrix} \quad (2.40) \end{aligned}$$

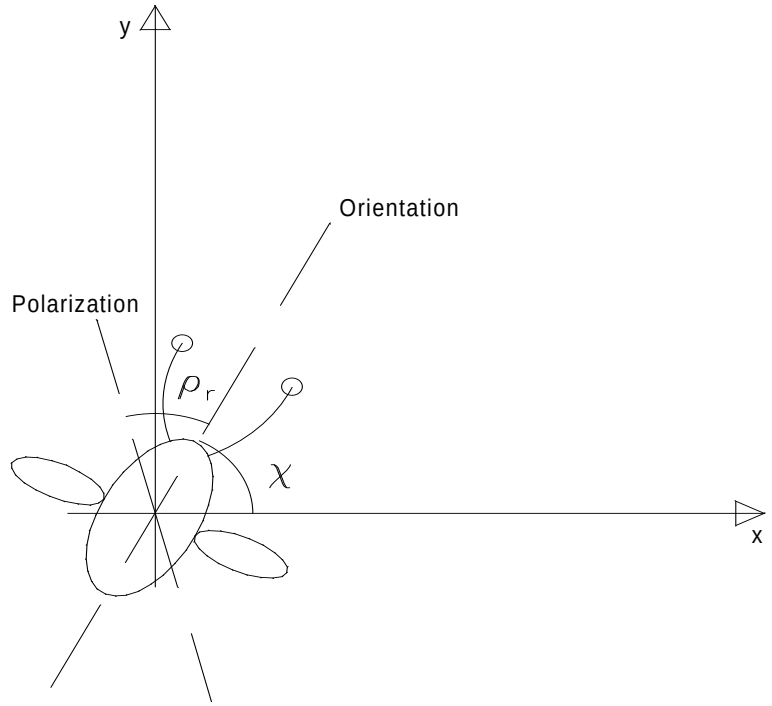

Figure 2.3: Target relative polarization ρ_r and the absolute orientation χ. The absolute polarization is $\rho = \rho_r + \chi$.

$$= \frac{\sigma_{xx}}{8}\left[\begin{array}{c} 3(1+\epsilon^2) + 2\epsilon\cos\beta + 4(1-\epsilon^2)\cos 2\rho_r \\ +(1 - 2\epsilon\cos\beta + \epsilon^2)\cos 4\rho_r \end{array}\right] \tag{2.41}$$

where the polarisation angle is given by

$$\begin{aligned} \rho &= \rho_0 + \omega t && (2.42)\\ &= \rho_r + \chi && (2.43)\\ \rho_r &= \rho_0 + \omega t - \chi && (2.44)\\ &= \rho_{r0} + \omega t && (2.45) \end{aligned}$$

Note that there are thus three parameters $(\sigma_{xx}, \epsilon, \beta)$ which describe the target's RCS (plus a parameter corresponding to the target's orientation relative to the polarisation direction at $t = 0$). Of these parameters, σ_{xx} is always positive. Solutions can be found such that ϵ lies between 0 and 1 (by forcing σ_{xx} to correspond to the strongest scattering orientation although this may not be parallel to an insect's body axis; in practice an assumption like this has to be made to obtain unambiguous results). The solution algorithm presented here does not limit ϵ to be less than 1, although this restriction can easily be applied to the raw results to remove any ambiguity (the orientation angle ρ_{r0} changes by $\pi/2$ to compensate). β lies between 0 and 180°(a fully polarimetric radar would allow β to be measured between 0 and 360°).

2.4 Complete System Model

The complete system model is obtained by combining the expressions for the beam shape and target RCS with Equation 2.2. The signal (p) is taken to be the natural log of the power ratio since this partially simplifies the analysis (the Gaussian beam shape becomes quadratic, but the RCS now has a ln term) and also because it better represents the output of radar receivers with a logarithmic output amplifier. Such receivers have a wide dynamic range and are thus appropriate for radar systems designed to cope with targets of different sizes at a large span of ranges, which is generally the case in radar entomology.

$$
\begin{aligned}
p(t) &= \ln\left(\frac{P_r}{P_{r0}}\right) && (2.46)\\
&= \ln\left(\frac{\sigma F^4 R_0^4}{\sigma_0 R^4}\right) && (2.47)\\
&= \ln\left(\frac{\sigma}{\sigma_0}\right) + 4\ln\left(\frac{R_0}{R}\right) + 4\ln F && (2.48)\\
&= \ln\left(\frac{\sigma_{xx}}{\sigma_0}\right) + 4\ln\left(\frac{R_0}{R}\right) \\
&\quad + \ln\left(\cos^4\rho_r + 2\epsilon\cos\beta\cos^2\rho_r\sin^2\rho_r + \epsilon^2\sin^4\rho_r\right) \\
&\quad + 4\left[\begin{array}{l} -\theta'^2(g_1 + g_2\cos 2\phi') \\ +2\theta'\theta''\left(g_1\cos\psi + g_2\cos(2\phi'+\psi)\right) \\ -\theta''^2\left(g_1 + g_2\cos 2(\phi'+\psi)\right)\end{array}\right] && (2.49)\\
&= c + \ln\left(\cos^4\rho_r + 2\epsilon\cos\beta\cos^2\rho_r\sin^2\rho_r + \epsilon^2\sin^4\rho_r\right) \\
&\quad -4\theta'^2(g_1 + g_2\cos 2\phi') + 8\theta'\theta''\left(g_1\cos\psi + g_2\cos(2\phi'+\psi)\right) \\
&\quad -4\theta''^2\left(g_1 + g_2\cos 2(\phi'+\psi)\right) && (2.50)
\end{aligned}
$$

where

$$c = \ln\left(\frac{\sigma_{xx}}{\sigma_0}\right) + 4\ln\left(\frac{R_0}{R}\right) \qquad (2.51)$$

The Gaussian beam approximation gives direct trigonometrical expressions for the beam shape terms when the signal is expressed as the logarithm of the power (as here), but all the other terms (including RCS parameters) are contained as logarithm values. The model is difficult (perhaps impossible) to invert analytically but relatively straightforward to invert numerically. Note that the signal variation due to position in the beam is likely to be stronger than that due to polarisation in general - position parameters will therefore often be easier to measure than RCS parameters.

Chapter 3

Solution Algorithm

The system model developed in the previous chapter is used to analyse measured signals from a nutating beam entomological radar. The model's parameters are adjusted using a standard non-linear optimisation algorithm to fit the model to the measured data. The goodness-of-fit between model and data, the best-fit model parameters and their covariances are the values calculated by the optimisation algorithm, and allow the insect's trajectory and radar cross-section parameters to be measured.

There are two main applications of the solution algorithm (system calibration and routine insect population monitoring) which are discussed in the next section. Implementation of the optimisation algorithm is described in the second section.

3.1 Applications of the Model

The complete system model has 14 parameters (Table 3.1), and can be used either to calibrate the system using a target with a known RCS (i.e. to measure those system parameters which are not easy to measure directly), or to measure the trajectory and RCS of an unknown target (e.g. general field experiments studying insect migration). Table 3.1 shows which parameters are fixed (i.e. assumed to be known *a priori*) and which are freed (to be found by model inversion) for the two cases of system calibration and routine insect monitoring.

When the model is to be inverted to estimate system parameters from measured data it is important to understand the model's characteristics. Since both the beam nutation and polarisation rotation are at the same frequency, signals due to both these effects may occur at the same frequencies (the fundamental (ω) and its harmonics), and the solution algorithm may have difficulty in distinguishing these two effects. For this reason, the model is appropriate for either calibrating the beam parameters using a known target, or for measuring the RCS and trajectory of an unknown target using a calibrated system, but is not suitable for attempting both simultaneously. Note that the constants σ_{xx} and R cannot be distinguished by the model and are treated as one combined variable c.

Parameter No.	Symbol	System Calibration	Field Operation	Remark
1	c			Range and σ_{xx}
2	x_0			Angular position at $t = 0$
3	y_0			
4	u			Angular velocity
5	v			
6	ϵ	set, $= 1$		RCS parameters
7	β	set, $= 0$		
8	θ'	set	set	Beam offset
9	ϕ'		set	Beam orientation
10	g_1		set	Beam shape parameters
11	g_2		set	
12	ρ_{r0}	set, $= 0$		Polarisation angle at $t = 0$ minus the target orientation
13	α_0	set	set	Beam centre azimuth at $t = 0$
14	ω	set	set	Nutation rate

Table 3.1: Model parameters free for different applications. (g_1 may be measured more reliably from the variation of the mean signal level during a beam transect with a known target than by direct model inversion.)

3.2 Implementing the Solution Algorithm

The model is non-linear and so an iterative algorithm is used to find the solution giving the best fit between the measured data and the model. The solution algorithm used at Cranfield is based on a maximum likelihood algorithm [4], which requires two types information in addition to the basic model described above, these are (1) the model partial derivatives with respect to the model parameters, and (2) a good first guess at the final solution. These are described in the following subsections.

3.2.1 Model Partial Derivatives

Using the notation of [4] the model parameters are the components of a 14 component vector **a**.

$$\begin{aligned} \frac{\partial p}{\partial a_1} &= \frac{\partial p}{\partial c} \\ &= 1 \end{aligned} \tag{3.1}$$

$$\begin{aligned} \frac{\partial p}{\partial a_2} &= \frac{\partial p}{\partial x_0} \\ &= \frac{\partial p}{\partial \theta''}\frac{\partial \theta''}{\partial x_0} + \frac{\partial p}{\partial \psi}\frac{\partial \psi}{\partial \phi''}\frac{\partial \phi''}{\partial x_0} \end{aligned} \tag{3.2}$$

$$\begin{aligned} \frac{\partial p}{\partial a_3} &= \frac{\partial p}{\partial y_0} \\ &= \frac{\partial p}{\partial \theta''}\frac{\partial \theta''}{\partial y_0} + \frac{\partial p}{\partial \psi}\frac{\partial \psi}{\partial \phi''}\frac{\partial \phi''}{\partial y_0} \end{aligned} \tag{3.3}$$

$$
\begin{aligned}
\frac{\partial p}{\partial a_4} &= \frac{\partial p}{\partial u} \\
&= \frac{\partial p}{\partial \theta''}\frac{\partial \theta''}{\partial u} + \frac{\partial p}{\partial \psi}\frac{\partial \psi}{\partial \phi''}\frac{\partial \phi''}{\partial u} && (3.4) \\
\frac{\partial p}{\partial a_5} &= \frac{\partial p}{\partial v} \\
&= \frac{\partial p}{\partial \theta''}\frac{\partial \theta''}{\partial v} + \frac{\partial p}{\partial \psi}\frac{\partial \psi}{\partial \phi''}\frac{\partial \phi''}{\partial v} && (3.5) \\
\frac{\partial p}{\partial a_6} &= \frac{\partial p}{\partial \epsilon} \\
&= 2\frac{\cos\beta\cos^2\rho_r\sin^2\rho_r + \epsilon\sin^4\rho_r}{\cos^4\rho_r + 2\epsilon\cos\beta\cos^2\rho_r\sin^2\rho_r + \epsilon^2\sin^4\rho_r} && (3.6) \\
\frac{\partial p}{\partial a_7} &= \frac{\partial p}{\partial \beta} \\
&= -2\frac{\epsilon\sin\beta\cos^2\rho_r\sin^2\rho_r}{\cos^4\rho_r + 2\epsilon\cos\beta\cos^2\rho_r\sin^2\rho_r + \epsilon^2\sin^4\rho_r} && (3.7) \\
\frac{\partial p}{\partial a_8} &= \frac{\partial p}{\partial \theta'} \\
&= -8.10^{-3} g_1\left[\theta' - \theta''\cos\psi\right] \\
&\quad -8.10^{-3} g_2\left[\theta'\cos 2\phi' - \theta''\cos(2\phi'+\psi)\right] && (3.8) \\
\frac{\partial p}{\partial a_9} &= \frac{\partial p}{\partial \phi'} \\
&= 8g_2\left[\theta'^2\sin 2\phi' - 2\theta'\theta''\sin(2\phi'+\psi) + \theta''^2\sin 2(\phi'+\psi)\right] && (3.9) \\
\frac{\partial p}{\partial a_{10}} &= \frac{\partial p}{\partial g_1} \\
&= -4\theta'^2 + 8\theta'\theta''\cos\psi - 4\theta''^2 && (3.10) \\
\frac{\partial p}{\partial a_{11}} &= \frac{\partial p}{\partial g_2} \\
&= -4\theta'^2\cos 2\phi' + 8\theta'\theta''\cos(2\phi'+\psi) - 4\theta''^2\cos 2(\phi'+\psi) && (3.11) \\
\frac{\partial p}{\partial a_{12}} &= \frac{\partial p}{\partial \rho_{r0}} \\
&= \frac{\partial p}{\partial \rho_r}\frac{\partial \rho_r}{\partial \rho_{r0}} \\
&= \frac{\partial p}{\partial \rho_r} \\
&= -\sin 2\rho_r\frac{1-\epsilon^2+\cos 2\rho_r(1-2\epsilon\cos\beta+\epsilon^2)}{\cos^4\rho_r + 2\epsilon\cos\beta\cos^2\rho_r\sin^2\rho_r + \epsilon^2\sin^4\rho_r} && (3.12) \\
\frac{\partial p}{\partial a_{13}} &= \frac{\partial p}{\partial \alpha_0} \\
&= \frac{\partial p}{\partial \psi}\frac{\partial \psi}{\partial \alpha_0} \\
&= -\frac{\partial p}{\partial \psi} \\
&= -8\theta''\left\{\theta'' g_2\sin 2(\phi'+\psi) - \theta'\left[g_1\sin\psi + g_2\sin(2\phi'+\psi)\right]\right\} && (3.13)
\end{aligned}
$$

$$\begin{aligned}
\frac{\partial p}{\partial a_{14}} &= \frac{\partial p}{\partial \omega} \\
&= \frac{\partial p}{\partial \rho_r}\frac{\partial \rho_r}{\partial \omega} + \frac{\partial p}{\partial \psi}\frac{\partial \psi}{\partial \omega} \\
&= t\left[\frac{\partial p}{\partial \rho_r} - \frac{\partial p}{\partial \psi}\right] \\
&= t\left[\frac{\partial p}{\partial a_{12}} + \frac{\partial p}{\partial a_{13}}\right] \qquad (3.14)
\end{aligned}$$

where

$$\begin{aligned}
\frac{\partial p}{\partial \theta''} &= 8\theta'\left[g_1\cos\psi + g_2\cos(2\phi'+\psi)\right] \\
&\quad -8\theta''\left[g_1 + g_2\cos 2(\phi'+\psi)\right] \qquad (3.15) \\
\frac{\partial p}{\partial \psi} &= -8\theta'\theta''\left[g_1\sin\psi + g_2\sin(2\phi'+\psi)\right] + 8\theta''^2 g_2\sin 2(\phi'+\psi) \qquad (3.16) \\
\frac{\partial \psi}{\partial \phi''} &= 1 \qquad (3.17) \\
\frac{\partial \theta''}{\partial x_0} &= \frac{\partial \theta''}{\partial x} \\
&= 10^{-3}\frac{x}{\theta''} \qquad (3.18) \\
\frac{\partial \theta''}{\partial y_0} &= \frac{\partial \theta''}{\partial y} \\
&= 10^{-3}\frac{y}{\theta''} \qquad (3.19) \\
\frac{\partial \theta''}{\partial u} &= 10^{-3}\frac{xt}{\theta''} \qquad (3.20) \\
\frac{\partial \theta''}{\partial v} &= 10^{-3}\frac{yt}{\theta''} \qquad (3.21) \\
\frac{\partial \phi''}{\partial x_0} &= \frac{\partial \phi''}{\partial x} \\
&= 10^{-3}\frac{-y}{\theta''^2} \qquad (3.22) \\
\frac{\partial \phi''}{\partial y_0} &= \frac{\partial \phi''}{\partial y} \\
&= 10^{-3}\frac{x}{\theta''^2} \qquad (3.23) \\
\frac{\partial \phi''}{\partial u} &= 10^{-3}\frac{-yt}{\theta''^2} \qquad (3.24) \\
\frac{\partial \phi''}{\partial v} &= 10^{-3}\frac{xt}{\theta''^2} \qquad (3.25)
\end{aligned}$$

Also

$$\begin{aligned}
\frac{\partial p}{\partial \gamma_1} &= \frac{\partial p}{\partial g_1}\frac{\partial g_1}{\partial \gamma_1} + \frac{\partial p}{\partial g_2}\frac{\partial g_2}{\partial \gamma_1} \\
&= \frac{4}{\gamma_1^3}\begin{bmatrix} \theta'^2(1+\cos 2\phi') + \theta''^2(1+\cos 2(\phi'+\psi)) \\ -2\theta'\theta''(\cos\psi + \cos(2\phi'+\psi)) \end{bmatrix} \qquad (3.26)
\end{aligned}$$

$$\begin{aligned}\frac{\partial p}{\partial \gamma_2} &= \frac{\partial p}{\partial g_1}\frac{\partial g_1}{\partial \gamma_2} + \frac{\partial p}{\partial g_2}\frac{\partial g_2}{\partial \gamma_2} \\ &= \frac{4}{\gamma_2^3}\left[\begin{array}{l}\theta'^2(1-\cos 2\phi') + \theta''^2(1-\cos 2(\phi'+\psi)) \\ -2\theta'\theta''(\cos\psi - \cos(2\phi'+\psi))\end{array}\right] \end{aligned} \tag{3.27}$$

using Equations 3.10, 3.11 and the following relationships

$$\frac{\partial g_1}{\partial \gamma_1} = \frac{-1}{\gamma_1^3} \tag{3.28}$$

$$\frac{\partial g_1}{\partial \gamma_2} = \frac{-1}{\gamma_2^3} \tag{3.29}$$

$$\frac{\partial g_2}{\partial \gamma_1} = \frac{-1}{\gamma_1^3} \tag{3.30}$$

$$\frac{\partial g_2}{\partial \gamma_2} = \frac{1}{\gamma_2^3} \tag{3.31}$$

3.2.2 First-Guess Values

Iterative solution methods must generally be initialised with good first-guesses of the desired solution if the solution is to be efficient and to avoid secondary minima. Table 3.2 lists the first-guesses used in the current solution algorithm. If some parameters are known *a priori* (for example from a previous calibration) then these values override the first-guess values.

The beam and trajectory parameters can be initialised using a quasi-static version of the system model assuming the target is a reflecting sphere (so that polarisation-dependent terms can be ignored). Equation 2.30 gives the parameters which can be measured directly this way using standard harmonic components of the signal. The following harmonic integrals (sums when implemented digitally) are used to provide estimates of the beam and trajectory parameters.

$$S_0 = \int_{\text{N rotations}} p\, dt \tag{3.32}$$

$$S_1 = \int_{\text{N rotations}} p\, \cos\omega t\, dt \tag{3.33}$$

$$S_2 = \int_{\text{N rotations}} p\, \sin\omega t\, dt \tag{3.34}$$

$$S_3 = \int_{\text{N rotations}} p\, \cos 2\omega t\, dt \tag{3.35}$$

$$S_4 = \int_{\text{N rotations}} p\, \sin 2\omega t\, dt \tag{3.36}$$

Comparing these integrals with the harmonic terms of Equation 2.30 for the simplified quasi-static model gives:

$$S_0 = \text{constant} - 4g_1\theta''^2 \tag{3.37}$$

$$S_1 = 4\theta'\theta''\left[g_1\cos(\phi'' - \alpha_0) + g_2\cos(2\phi' + \phi'' - \alpha_0)\right] \tag{3.38}$$

$$S_2 = 4\theta'\theta''\left[g_1\sin(\phi'' - \alpha_0) + g_2\sin(2\phi' + \phi'' - \alpha_0)\right] \tag{3.39}$$

$$S_3 = -2\theta''^2 g_2\cos 2(\phi' + \phi'' - \alpha_0) \tag{3.40}$$

$$S_4 = -2\theta''^2 g_2\sin 2(\phi' + \phi'' - \alpha_0) \tag{3.41}$$

(Note that if the target moves uniformly across the beam, and slowly enough for the quasi-static model to apply, then S_0 depends quadratically on θ''. This can be used to measure g_1 in a suitable calibration experiment.)

Thus first-guess values using this simplified quasi-static model are:

$$\theta'' = \frac{\sqrt{S_1^2 + S_2^2}}{4\theta' g_1} \quad \text{(assuming } g_1 \gg g_2\text{)} \tag{3.42}$$

$$\phi'' = \alpha_0 + \tan^{-1}(S_2/S_1) \tag{3.43}$$

$$g_2 = \frac{\sqrt{S_3^2 + S_4^2}}{S_1^2 + S_2^2} 4\theta'^2 g_1^2 \tag{3.44}$$

$$\phi' = \frac{1}{2}\tan^{-1}\left(\frac{-S_4/(2g_2\theta''^2)}{-S_3/(2g_2\theta''^2)}\right) - (\phi'' - \alpha_0) \tag{3.45}$$

Values for x_0 and y_0 follow from the values for θ'' and ϕ'', and u, v are both taken to be zero.

The target RCS parameters are guessed using values which are typical of the expected targets and which avoid points in the model where gradients tend to zero or infinity. If the beam parameters are known it is possible to obtain improved estimates of the RCS parameters using an iterative procedure, but this adds significantly to the complexity of the algorithm for deriving the *first-guess* values, and should not significantly affect the accuracy of the final solution.

3.2.3 Achieving a Practical Implementation

The above equations can be implemented directly as indicated [4] but may not work satisfactorily due to the nature of the numerical solution. The following steps have been found to give a relatively robust solution algorithm.

1. The magnitudes of the partial derivatives of the model with respect to its parameters should not differ too greatly from each other (to give a better posed problem for numerical solution). To help this, the parameter units need not be standard SI units; in this case the angular positions and speeds have been expressed using mrad rather than rad.

2. Matrix inversion routines are required at several stages of the solution. Singular value decomposition (SVD) methods are used (implemented in double precision) at Cranfield and give a robust algorithm able to test for (and warn against) near singular cases (indicating inadequate measurements for the parameter estimation being attempted).

3.3 Interpreting χ^2

The χ^2 statistic calculated using the solution algorithm has the great advantage that it can be interpreted quantitatively [4] (if the measurement noise σ_i is properly calibrated). An additional statistic against which χ^2 can be compared is χ_0^2, which is defined using the (weighted) mean of the signal as the model "fitted" to the data.

Parameter				First Guess Remarks
No.	Symbol	Unit	Quantity	
1	c	none	$\ln(\frac{\sigma_{xx}}{\sigma_0}) + 4\ln(\frac{R_0}{R})$	measure R, guess σ_{xx} according to local conditions
2	x_0	mrad	x at $t = 0$	use simplified quasi-static model
3	y_0	mrad	y at $t = 0$	use simplified quasi-static model
4	u	mrad s^{-1}	target angular velocity (x)	use simplified quasi-static model
5	v	mrad s^{-1}	target angular velocity (y)	use simplified quasi-static model
6	ϵ	none	$\sqrt{\sigma_{yy}/\sigma_{xx}}$	0.8 (arbitrary choice)
7	β	rad	target RCS relative phase	0.2 (arbitrary choice)
8	θ'	rad	beam offset (radial)	antenna measurement / beam deviation factor
9	ϕ'	rad	beam offset (azimuth)	from quasi-static model (check against antenna measurement)
10	g_1	rad^{-2}	∼mean beam diameter	Use nominal beamwidth of aperture $\gamma_1 = \gamma_2$ from equation 2.11 or calibrate (Eq. 3.32)
11	g_2	rad^{-2}	∼beam ellipticity	from quasi-static model
12	ρ_{r0}	rad	$\rho_r - \chi$ at $t = 0$	antenna measurement at antenna head-up position
13	α_0	rad	α at $t = 0$	define $\alpha_0 = 0$ at head-up position
14	ω	rad s^{-1}	nutation rate	10 rev $s^{-1} = 20\pi$ rad s^{-1}; Cranfield / USDA system measures signal at fixed angular steps ($2\pi/256$ rad) so that ω is not a parameter

Table 3.2: First-Guess Values used in the solution algorithm ($t = 0$ is defined here as time at the "head-up" position).

$$\chi_0^2 = \sum \left(\frac{y_i - \overline{y}}{\sigma_i} \right)^2 \tag{3.46}$$

where

$$\overline{y} = \frac{\sum \frac{y_i}{\sigma_i}}{\sum \frac{1}{\sigma_i}} \tag{3.47}$$

If the signal is strong then χ^2 and χ_0^2 should differ significantly (because the model fits the data much better than a simple average), but if noise dominates then χ^2 and χ_0^2 will differ only by the difference in the number of degrees of freedom between the mean (1 degree of freedom) and the model.

In practice these statistics are useful either to improve understanding of the measurement noise (mis-calibration of the noise model will be revealed by unexpected values of χ^2), or to give quantitative information about the goodness-of-fit of the model to the data and the signal-to-noise ratio of the data.

Chapter 4

Demonstration Results

Examples of results using the analysis methods described above are given in this section to illustrate their capability when applied to real data. The results are not presented as fully calibrated measurements but only to illustrate application of the model and algorithms described in earlier chapters.

Note that the analysis has been performed using a system model with 12 parameters, not the full 14 parameters given in the previous chapters (because the rotation rate ω is taken to be constant and the position coordinates are relative to dipole position at $t = 0$, i.e. $\alpha_0 = 0$ can be assumed). The data have all been analysed in sections of 512 readings, i.e. 0.2 s of data, or 2 dipole revolutions. Neighbouring points are 0.1 s apart, and thus have half their data in common.

4.1 Field Experiments (November 1988)

Field experiments using the U.S. Department of Agriculture (USDA) X-band entomological radar with nutating beam and the Cranfield signal acquisition unit took place in November 1988 [5]. Two types of measurement were made: (1) radar system calibrations using a steel sphere of known RCS, and (2) routine insect monitoring with the beam pointing vertically upwards.

The radar wavelength is 3.2 cm (X-band), its pulse repetition frequency is 2560 Hz, and the antenna is an offset Cutler feed rotating at 10 Hz in a circular reflector of diameter 0.6 m.

The signal acquisition unit uses a manual range control and data are recorded using a microcomputer (Apple II) with 12-bit ADC inputs able to record for 4.8 s (48 antenna revolutions). These data have been transferred to standard PC format for analysis. In all the cases presented here the data have been analysed in sections of 0.2 s duration (i.e. 2 dipole revolutions). Longer or shorter periods could be used, but it is recommended that at least one revolution is used to give a complete span of measurements.

4.1.1 Pre-processing of the Raw Data

The available data are stored as DN values corresponding to the ADC output. These data need to be converted into power ratio units to obtain $p(t)$. In

addition to p, corresponding values of t and $\sigma(p)$ also need to be provided. For the Cranfield / USDA system, the independent variable is nutation angle rather than time ($\omega t = n.2\pi/256$ rad), and ω is no longer a system parameter. Angle is converted directly to time assuming a dipole rotation rate of exactly 10 Hz.

4.1.2 System Noise Model

A noise model had to be developed to estimate $\sigma(p)$. The model used assumes the noise level is a function of the signal level. The model was based on the measured data by subjectively fitting a model to the observed standard deviation variation with mean signal level for short data windows, and then calculating $\sigma(p)$ using this model for each record based on the apparent power measured. With more extensive operating experience it should be possible (and would be desireable) to develop a more comprehensive and validated noise model.

The noise model used for the results presented here was satisfactory for demonstrating application of the algorithms but was not accurate enough for quantitative interpretation of the goodness of fit measure (or the parameter error covariances). If anything, the goodness of fit measure obtained can be used to improve the noise model to give more typical results (i.e. the χ^2 value for the fit of the model to the data should be approximately equal to the number of degrees of freedom). Similarly, the error covariances are not correct, although their general magitudes and relative values are good.

Figure 4.8 shows the χ^2 achieved using the current noise model. If the model were correct then the fitted value would be approximately 500 (the number of degrees of freedom of the data less the number of degrees of freedom of the model). These results suggest that the actual measurement noise is smaller than modelled for small signals and larger than modelled for large signals.

4.2 Radar System Calibration

The principal objective of the system calibration experiments was to measure relevant beam parameters (e.g. g_1, g_2). A steel sphere was used as the radar target, suspended part way along the tether line of a helium-filled balloon. Using the motorised antenna mount, the radar beam was scanned across the target in both elevation and azimuth. The data presented are from signal recorded for a transect referred to as RD34 for which the raw data are relatively strong.

Beam shape parameters were measured from the variation of mean power with scan angle (g_1, equation 3.37) and by model inversion (g_2, ϕ'). Examples of raw and analysed data are shown in figures 4.1 to 4.6. The target locus is measured well. The scatter in beam parameter estimates is broader than the maximum likelihood covariance estimates (equivalent standard deviations approximately $\pm$ 0.83°for $a[9] = \phi'$, $\pm$3.9 for $a[11] = g_2$) and is probably due to side-lobe interference (the target was only just above elevations clearly contaminated by ground clutter). If g_1 is attempted to be estimated by model inversion then the equations are almost degenerate (only θ' sets the angular scale size) and poor results are obtained.

4.3 Field Observations

Although not part of a coordinated field campaign, the radar was set for routine data collection with the beam vertical to record data for a set of real (almost certainly insect) targets. The data presented are from signal recorded as file RD17. The signal strength is reasonable for the first 2.5 s but then the target appears to have left the beam.

Figures 4.7 to 4.13 show the results for one of the targets observed. The locus appears to be measured accurately for the first 2.5 s (while the signal strength is good). The radial excursion at ∼1.0 s corresponds well with the dip in signal power. The target RCS parameters measured during the period of closest approach ($t = 1.5 - 2.0$ s) are relatively stable and could be used to classify the target or estimate its mass (using σ_{xx}). Figure 4.10 shows that the target passed through the edge of the beam, and thus its position parameters are not easy to estimate accurately. The results suggest that orientation may be easier to measure than position since the scatter in Figure 4.13 is relatively low (especially if the ambiguity which couples ϵ and ρ_{r0} is resolved).

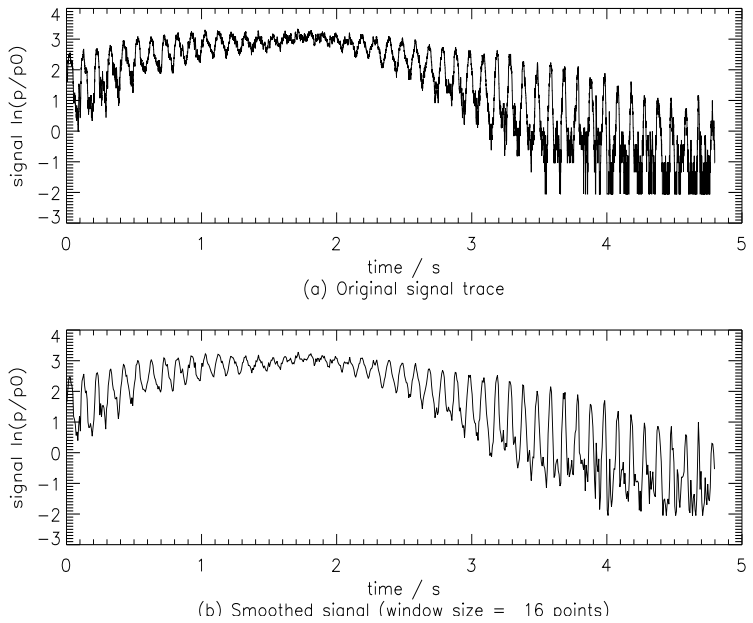

Figure 4.1: RD34 signal trace (raw and with moderate filtering to show the main features). The signal is expressed in natural log units of the power. 256 data points are recorded per dipole revolution (0.1 s).

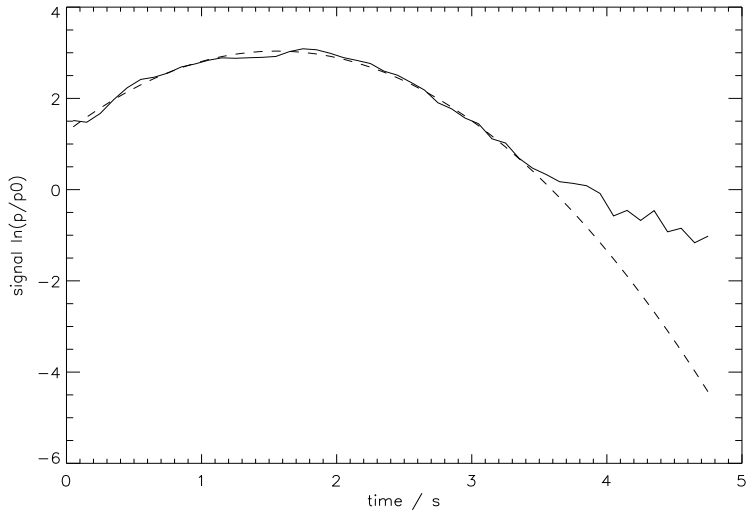

Figure 4.2: RD34 mean power. The envelope should be parabolic for a uniform sweep of the beam across the target (the dashed line shows a best-fit parabola for the main part of the trace used to estimate the beam width parameter g_1).

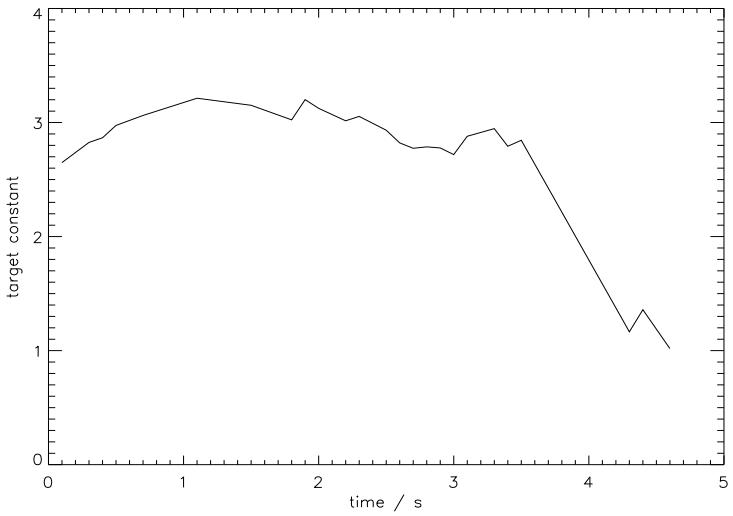

Figure 4.3: RD34 target constant. Variations are probably due to sidelobe interference or to slight changes in range.

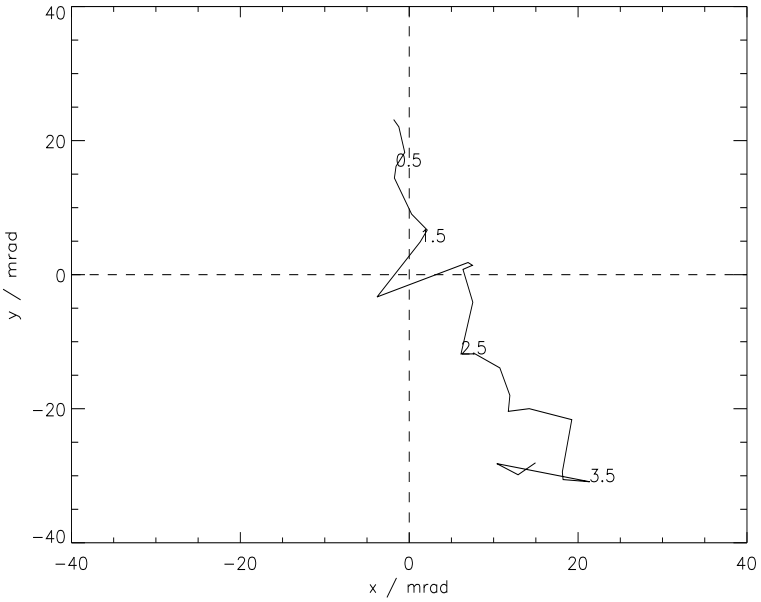

Figure 4.4: RD34 estimated target locus. 1 mrad is equivalent to 0.43 m (target range = 430 m); the beam centre is displaced 13.4 mrad from the coordinate origin. Times of measured positions are shown for $t = 0.5 - 3.5$ s.

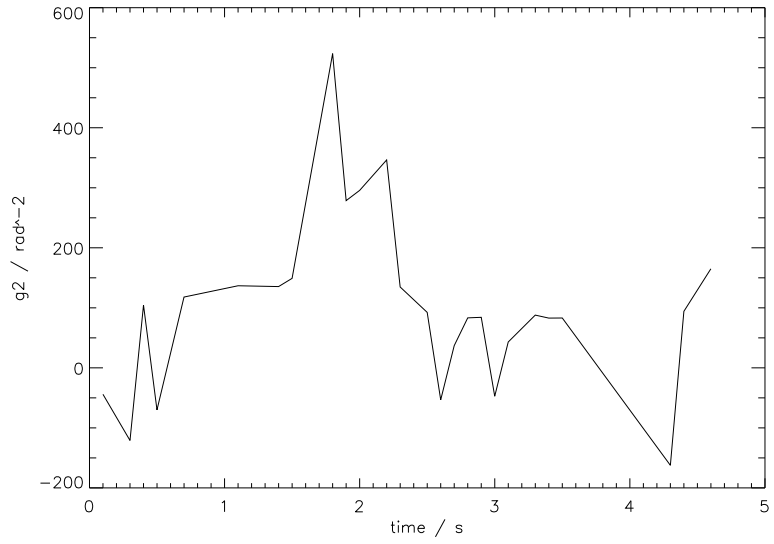

Figure 4.5: RD34 beam ellipticity parameter g_2 estimated at various times through the signal.

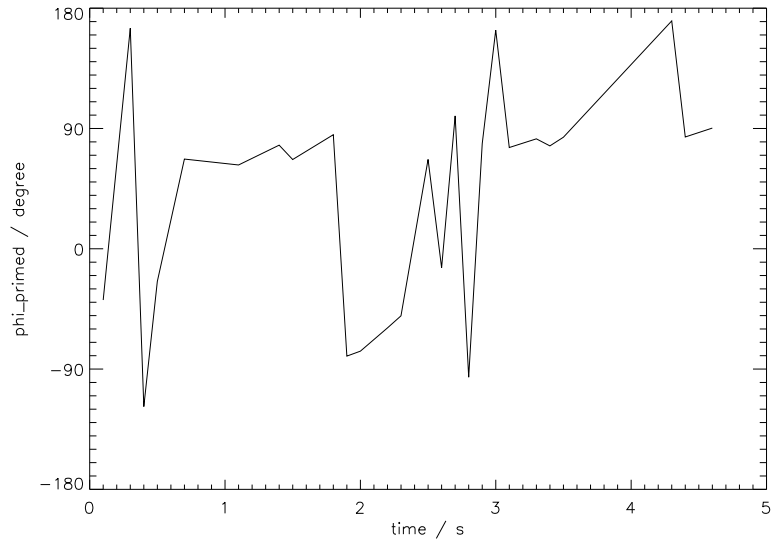

Figure 4.6: RD34 beam azimuth parameter ϕ' estimated at various times through the trace.

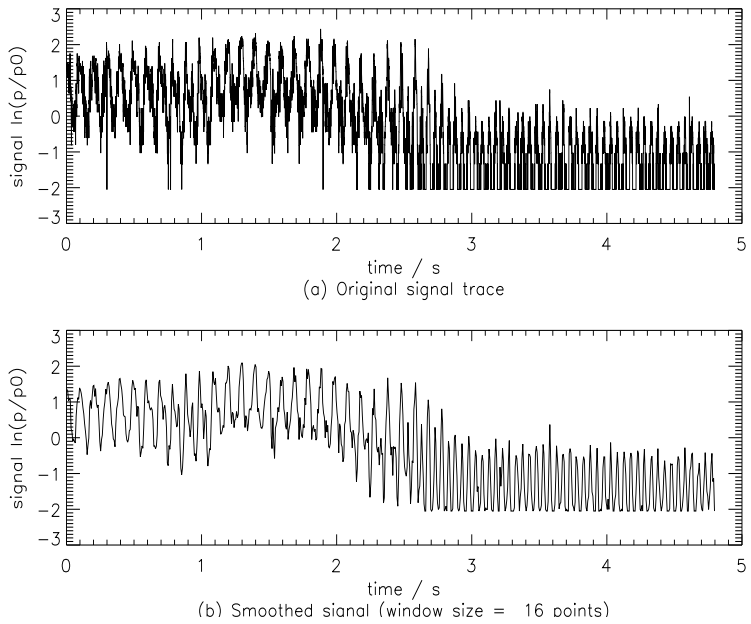

Figure 4.7: RD17 signal (raw and with moderate filtering to show the main features). The signal is expressed in natural log units of the power. 256 data points are recorded per dipole revolution (0.1 s).

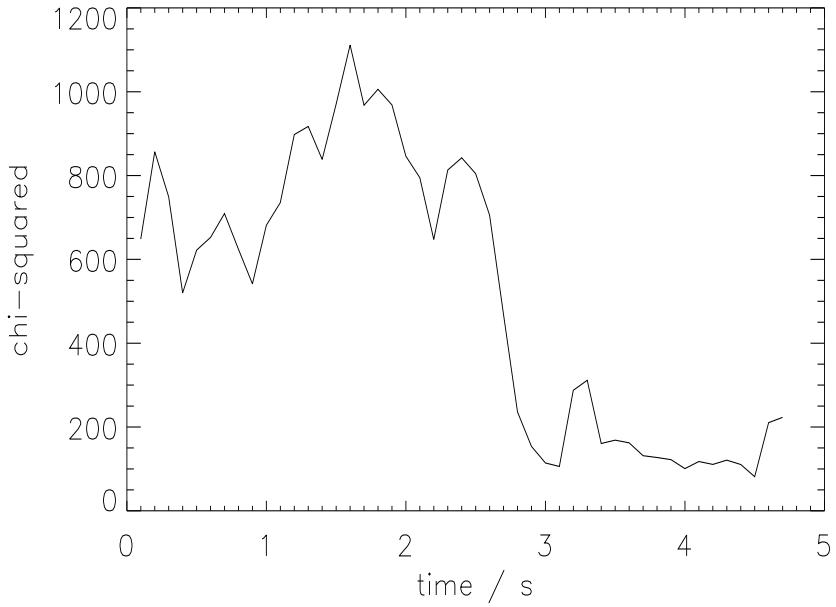

Figure 4.8: RD17 χ^2 for the fitted model. The model was fitted using data for 0.2 s (two dipole revolutions) and repeated at 0.1 s steps; adjacent points thus have 1 revolution of data in common.

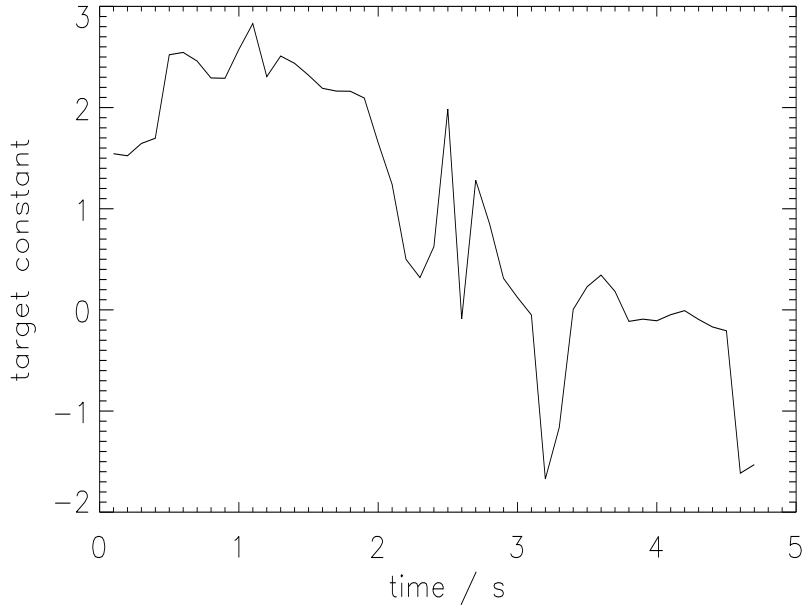

Figure 4.9: RD17 target constant estimated as a function of time.

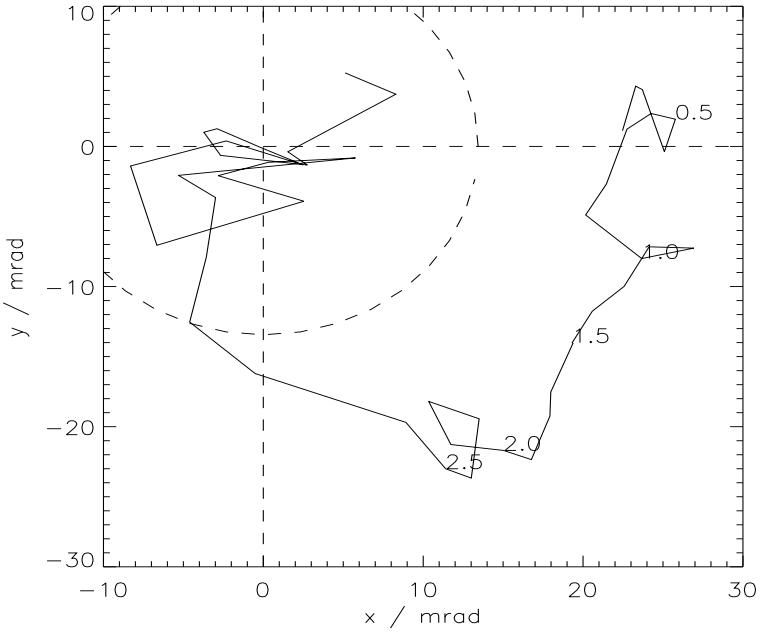

Figure 4.10: RD17 estimated target locus. The beam centre locus is shown by the dashed arc, and the times at which positions were recorded are noted for $t = 0.5 - 2.5$ s. 1 mrad is approximately 0.60 m in lateral distance (range is about 600 m).

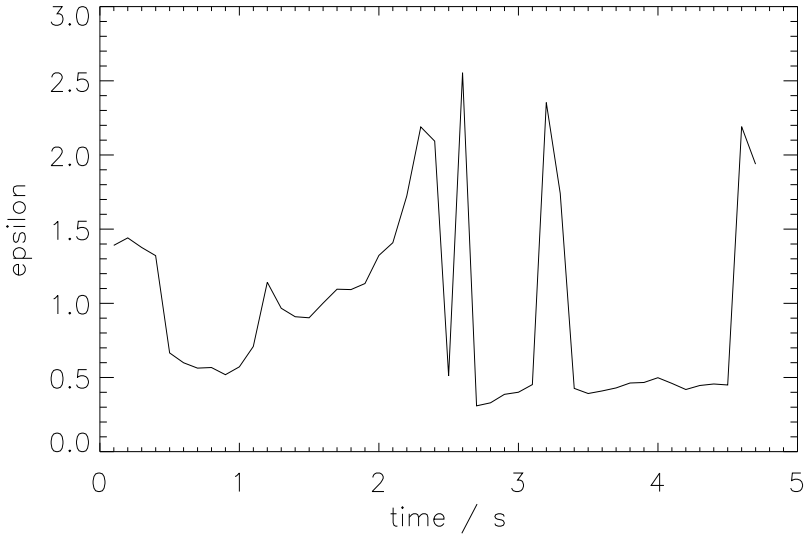

Figure 4.11: RD17 target radar cross-section parameter ϵ estimated from the recorded signal. The fluctuations around $\epsilon = 1$ correlate with apparent changes in orientation ρ_{r0} as expected.

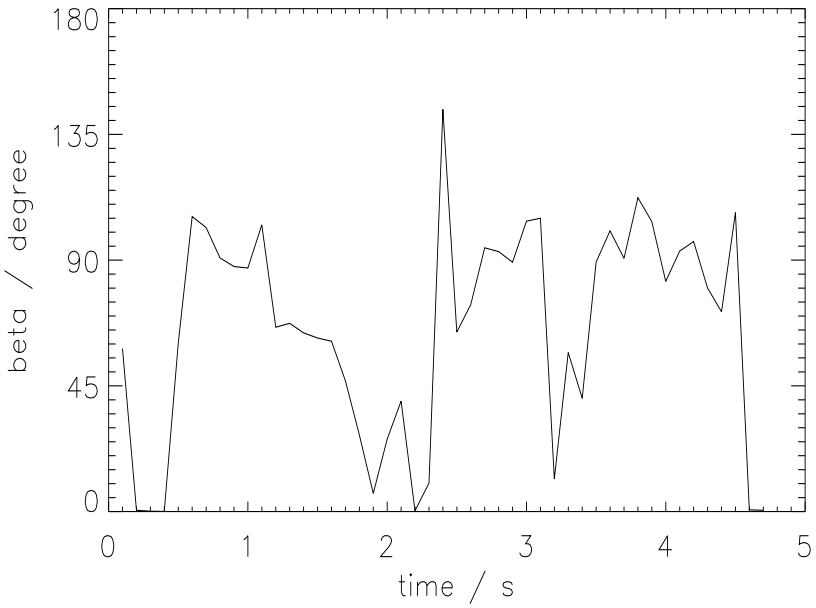

Figure 4.12: RD17 target radar cross-section parameter β (degrees) estimated at various times during the sample.

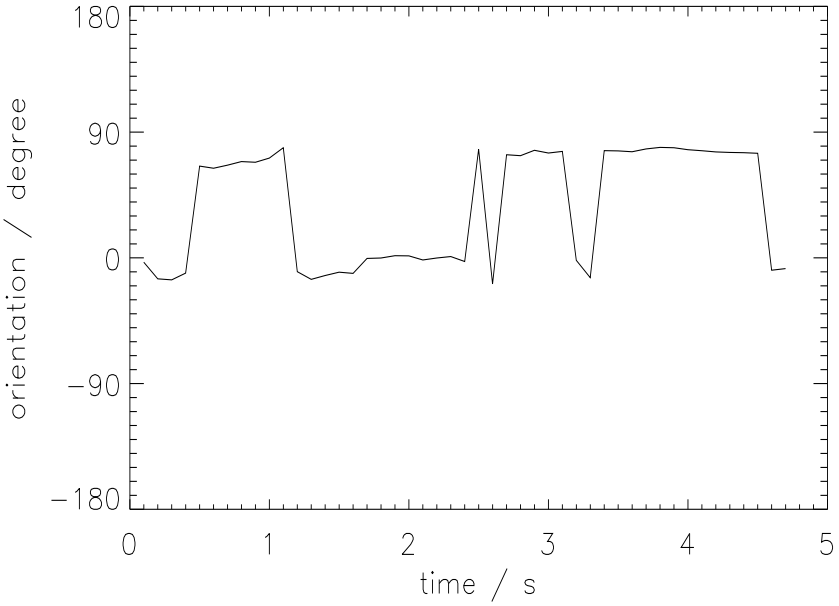

Figure 4.13: RD17 target orientation ρ_{r0} (degrees) estimated from the recorded signal. Note the bimodal distribution (which correlates with changes in ϵ).

Chapter 5

Discussion and Conclusions

Developing the radar system model, implementing it and the solution algorithm on a microcomputer, and then applying it to real field data has been a valuable exercise. The following sections consider the most significant features of the project.

5.1 Discussion

The results suggest that the model and solution methods can be applied practically and can provide useful results. The direct results presented here clearly have to be interpreted carefully. The quantification of goodness-of-fit and of the random noise induced parameter uncertainties make the identification of biases and systematic errors (e.g. side-lobe interference) relatively unambiguous, even in this example with a poor system noise model, which is a significant strength.

A major source of error with the system used to obtain the field data is the radar system's sensitivity to target range. This is because the transmitted radar pulse does not have a flat power profile and the signal acquisition uses sample-hold devices which sample the "instantaneous" signal (a peak detector with a flat range response within a controllable range gate would avoid this difficulty). Much of the apparent variation in target parameters is assumed to be due to this range sensitivity.

The beam shape parameters are inadequately measured using the current data. Side-lobe interference is the most plausible explanation of the observed scatter, especially its apparently systematic variation (e.g. Fig. 4.5). The target parameters are, if anything, more convincing (possibly because the vertical beam orientation is less prone to side-lobe interference). There is a clear correlation between the signal strength (Fig. 4.7) and position (Fig. 4.10), and parameters estimated during the period of closest approach to beam centre ($t = 1.5 - 2.0s$) are relatively stable. Given the measured target range of 598 m, the system constant of 3.1 ± 0.2 for the reference target ($R_0 = 430$ m, $\sigma_{xx} = 2.51cm^2$), the apparent target value of σ_{xx} is $3.8cm^2$. This corresponds to an insect of mass approximately 1 g [6].

The model has wider use than the data analysis demonstrated here. An example application is as a parametric model allowing the radar system design to be optimised for specific purposes.

5.2 Conclusions

This report presents a model applicable to current nutating beam entomological radars. The model is relatively comprehensive (and includes non-circular beam cross-section, target RCS described by three parameters, and (linear) target velocity). An implementation of the model to allow parameter estimation from measured data for either (1) system calibration, or (2) insect monitoring, is described. The method is demonstrated on actual radar data collected in field experiments for the U.S. Department of Agriculture, and shows promising results.

Particular strengths of the method are (1) the sophistication of the underlying model, and (2) the solution algorithm's ability to quantify goodness-of-fit and the parameter errors. Further work is required to develop methods of automatically processing the direct results (e.g. identifying data portions giving the most reliable parameter estimates) to enable routine insect monitoring. It is also clear that increasing the power of the data analysis places greater demands on the quality of the calibration of the radar system (i.e. an accurate system noise model is required). These are achievable objectives and it is feasible to consider an automated insect monitoring system based on the techniques described here.

Bibliography

[1] Smith, A.D., Riley, J.R., and Gregory, R.D.: 1993, A method for routine monitoring of the aerial migration of insects by using a vertical-looking radar, *Phil. Trans. R. Soc. Lond. B* **Vol. 340**, pp. 393–404.

[2] Ulaby, F.T., Moore, R.K., and Fung, A.K.: 1981, *Microwave Remote Sensing Volume 1*, Artech House Inc.: Norwood, MA, USA, 456 pp.

[3] Skolnik, M.I.: 1970, *Radar Handbook*, McGraw-Hill Book Company, New York, 1536 pp.

[4] Press, W.H., Teukolsky, S.A., Vetterling, W.T., and Flannery, B.P.: 1992, *Numerical Recipes in C, Second Edition*, Cambridge University Press: Cambridge, 994 pp.

[5] Hobbs, S.E.: 1989, *Signal Analysis for Entomological Radar, Final Report, August 1989*, School of Industrial Science, Cranfield Institute of Technology. (Refer to the principal author or U.S. Department of Agriculture, Mr. W. Wolf, for details of this contract report.)

[6] Aldhous, A.C.: 1989, *An investigation of the polarisation dependence of insect radar cross-sections at constant aspect.* PhD Thesis, Cranfield Institute of Technology, Cranfield, 167 pp.

Appendix A

Data Processing of the Cranfield / USDA Experiments

The experiment organisation and data collection as far as obtaining data files on an Apple II microcomputer are described in a contractor report [5] available from the authors. These data have been transferred to a PC compatible microcomputer (using a standard serial communications link, transferring the files as a string of ASCII characters) for the analysis presented here.

The main data processing and analysis stages are

- Collect radar data (program GBR1.1bgs running on the Apple II).
- Transfer raw data as ASCII files (printed by program GBR1.1bgs) over a serial communication link between computers.
- Convert the raw data (received as digital number values from the ADC output) to the format required by the maximum likelihood model fitting program (conversion performed by program filtrec.exe).
- Analyse the correctly formatted data (analysis performed by program mfitgbr.exe).

An example of the raw data digital number (DN) values from the ADC as received by the PC is given in Table A.1, and the same data are shown in Table A.2 converted ready for analysis.

A.1 System Calibration

The conversion from DN to voltage (accounting for ADC scaling and the sample-hold gain, etc.) is given by

$$V = 2.714DN/255 \text{ (gives voltage in V)} \tag{A.1}$$

The calibration is approximately 10.6 mV per DN.

The calibration of the radar receiver signal (p, the natural logarithm of the signal power (P) in units of a reference power level P_{ref} near the system noise level) as a function of receiver video voltage (V, volts) is

$$p = 0.1 \ln 10(30.2529\sqrt{V} - 8.8978) \text{ for } V \leq 0.3432V \quad \text{(A.2)}$$
$$= 0.1 \ln 10(21.3446\sqrt{V} - 3.6789) \text{ for } V > 0.3432V \quad \text{(A.3)}$$

(The factor $0.1 \ln 10$ converts the calibration from decibels to the natural logarithm value.)

A.2 System Noise Model Used

The noise model giving absolute (not ln) signal noise (in units of the reference power level P_{ref}) as a function of the radar video output voltage (V) is

$$\sigma(V) = 0.3 \text{ for } V \leq 0 \quad \text{(A.4)}$$
$$= 0.3 + 0.7V/0.3 \text{ for } 0 < V \leq 0.3V \quad \text{(A.5)}$$
$$= 1.0 \text{ for } 0.3V \leq V \quad \text{(A.6)}$$

This absolute noise level is converted to the equivalent ln value by calculating the signal level $P(V) = \exp p(V)$ and the noise level $\sigma(V)$ for a given signal voltage, and then calculating the value $\delta p = \ln(1 + \sigma/P)$.

Results presented in this report suggest that this noise model is too large for low signals and too small for large signals.

GBR88 raw data, rd17 From data file #9:rd17, records 0 to 47

rev	angle	SH0	SH1	check_sum
0	0	22	7	29
0	1	22	7	29
0	2	23	9	32
0	3	22	3	25
0	4	22	3	25
0	5	22	11	33
0	6	21	6	27
0	7	21	2	23
0	8	23	2	25
0	9	23	5	28
0	10	23	6	29
0	11	22	8	30
0	12	23	6	29
0	13	24	9	33
0	14	23	7	30
0	15	23	6	29

Table A.1: A sample of the raw ASCII data transferred from Apple II to PC for file RD17 (data for the first 16 signals recorded by each sample-hold are shown). The columns are dipole revolution number, dipole rotation (counts from 0 to 255 over one revolution), ADC reading for the two sample-holds, and a check-sum (the total of the two sample-hold readings).

0.0000	1.3220	0.2035
0.0245	1.3220	0.2035
0.0491	1.3977	0.1950
0.0736	1.3220	0.2035
0.0982	1.3220	0.2035
0.1227	1.3220	0.2035
0.1473	1.2445	0.2124
0.1718	1.2445	0.2124
0.1963	1.3977	0.1950
0.2209	1.3977	0.1950
0.2454	1.3977	0.1950
0.2700	1.3220	0.2035
0.2945	1.3977	0.1950
0.3191	1.4719	0.1870
0.3436	1.3977	0.1950
0.3682	1.3977	0.1950

Table A.2: Signal from the first sample-hold (SH0) of the first 16 records of file RD17.txt (as in Table A.1) converted ready for input to mfitgbr.exe. The columns are dipole angle (radians), signal (ln(P/Pref)) and estimated uncertainty for the signal.

Appendix B

Data Analysis Cases

Two particular sets of recorded data have been analysed to generate the results presented in this report. The cases are referred as RD17 and RD34 (being the 17th and 34th data traces recorded in the Cranfield / USDA field experiments).

The parameter settings used to obtain the results in these two cases are given in Tables B.1 and B.2. RD34 is a beam profile calibration transect and RD17 contains signal recorded for an unknown target which is probably an insect of mass approximately 1 g.

Note that in both these cases the data analysis model has only 12 parameters, not the full 14 described earlier in the report (for the Cranfield / USDA system the dipole rotation rate is fixed and the position coordinates are relative to the head-up direction, i.e. $\alpha_0 = 0$).

Parameter number	Remark
1	Parameter free
2	Parameter free
3	Parameter free
4	Parameter free
5	Parameter free
6	Parameter free
7	Parameter free
8	$\theta' = 0.01344$ rad
9	$\phi' = 1.5708$ rad
10	$g_1 = 380$ rad^{-2}
11	$g_2 = 85$ rad^{-2}
12	Parameter free

Table B.1: The model parameter values used to obtain results from file RD17z.txt.

Parameter number	Remark
1	Parameter free
2	Parameter free
3	Parameter free
4	Parameter free
5	Parameter free
6	$\epsilon = 1.0$
7	$\beta = 0.0$
8	$\theta' = 0.01344$ rad
9	Parameter free
10	$g_1 = 380$ rad^{-2}
11	Parameter free
12	$\rho_{r0} = 0$

Table B.2: The model parameter values used to obtain results from file RD34z.txt.